In vivo Targeting of Dead Tumor Cells in a Murine Tumor Model Using a Monoclonal Antibody Specific for the La Autoantigen

Fares Al-Ejeh,[1] Jocelyn M. Darby,[1] Katherine Pensa,[1] Kerrilyn R. Diener,[1] John D. Hayball,[1,2] and Michael P. Brown[1,3]

Abstract

Purpose: To investigate the potential of the La-specific monoclonal antibody (mAb) 3B9 as an *in vivo* tumor-targeting agent.

Experimental Design: The murine EL4 lymphoma cell line was used for *in vitro* studies and the EL4 model in which apoptosis was induced with cyclophosphamide and etoposide was used for *in vivo* studies. *In vitro* studies compared 3B9 binding in the EL4 cell with that in its counterpart primary cell type of the thymocyte. For *in vivo* studies, 3B9 was intrinsically or extrinsically labeled with carbon-14 or 1,4,7,10-tetra-azacylododecane-N,N',N'',N''''-tetraacetic acid – indium-111, respectively, and biodistribution of the radiotracers was investigated in EL4 tumor-bearing mice, which were treated or not with chemotherapy.

Results: La-specific 3B9 mAb bound EL4 cells rather than thymocytes, and binding was detergent resistant. 3B9 binding to dead EL4 cells *in vitro* was specific, rapid, and saturable. Significantly, more 3B9 bound dead EL4 tumor explant cells after host mice were treated with chemotherapy, which suggested that DNA damage induced 3B9 binding. Tumor binding of 3B9 *in vivo* was antigen specific and increased significantly after chemotherapy. Tumor accumulation of 3B9 peaked at ∼50% of the injected dose per gram of tumor 72 h after chemotherapy and correlated with increased tumor cell death. Tumor/organ ratios of 3B9 biodistribution, which included the tumor/blood ratio, exceeded unity 48 or more hours after chemotherapy.

Conclusions: La-specific mAb selectively targeted dead tumor cells *in vivo*, and targeting was augmented by cytotoxic chemotherapy. This novel cell death radioligand may be useful both for radioimmunoscintigraphy and radioimmunotherapy.

Radioimmunoscintigraphy is a useful diagnostic imaging modality for both tumor detection and monitoring response to antitumor therapies. Although evasion of apoptosis is recognized as a hallmark of cancer (1), as tumors grow and outstrip their blood supply, dead cells remain a common feature of many malignancies (2). Moreover, breast tumor biopsies done before and after patients were given their first cycle of neoadjuvant chemotherapy indicated that many subsequently responding tumors displayed a treatment-related increase in content of apoptotic cells (3 – 5), which validates the apoptotic cell as a target for evaluating chemoresponsiveness. Fluorodeoxyglucose-positron emission tomography is a widely available technology that has an emerging role in tumor response evaluation (6). However, the need for indices of tumor biology other than metabolic activity has driven the search for other radioligands, in particular those that are selective for cell death (7). Preclinical and clinical studies using Annexin V, which binds phosphatidylserine both in the interior of necrotic cells and when externalized on the outer cell surface during apoptosis, identified dead tumor cells *in vivo* (8 – 11), which increased significantly in number after treatment with cytotoxic chemotherapy (8, 9, 11, 12). Nevertheless, clinical studies showed that the ^{99m}Tc-labeled version of Annexin V inconsistently detected cell death responses to chemotherapy. The short circulatory half-life of ^{99m}Tc-HYNIC-Annexin V and the indeterminate timing of cell death in human carcinoma after cytotoxic chemotherapy made it difficult to correlate tumor uptake of the reagent with tumor response (13).

There are several Food and Drug Administration – approved and marketed radioimmunoscintigraphy products, which include arcitumomab (CEAScan), imciromab (Myoscint), and capromab (Prostascint). Although arcitumomab recognizes a cell surface antigen, both imciromab and capromab bind intracellular epitopes, which requires cell permeability. Imciromab binds myosin heavy chain in necrotic muscle cells and was approved for detection of myocardial infarction. However, although imciromab efficiently detected necrotic muscle 6 days or more after the ischemic event (14 – 16), its utility in the clinical management of acute infarction has not been well defined. Interestingly, radiolabeled anti-myosin (Fab)$_2$ fragments detected necrotic soft tissue sarcomas *in vivo* regardless

of whether the tumors expressed myosin (17). Capromab binds an epitope located in the cytoplasmic domain of prostate-specific membrane antigen and, hence, preferentially detected necrotic cells, which was shown in tumor xenograft models (18). Nevertheless, in metastatic prostate cancer patients, many of the radiologically discernable lesions were not imaged using capromab (19). Investigational imaging agents have also been used to detect dead cell ghosts and extracellular products of dead cells. Tumor necrosis therapy is a novel approach to radioimmunoscintigraphy and radioimmunotherapy (20), which uses a monoclonal antibody (mAb) specific for histones and ssDNA that bind in necrotic and degenerating regions of tumors (20–22). In a pivotal registration study resulting in Chinese Food and Drug Administration approval for the first radioimmunotherapy for carcinoma, 107 patients with locally advanced and metastatic lung cancer were given ^{131}I-labeled chimeric TNT mAb, which produced an overall response rate of 35% although overall survival differed little from historical controls (23). Insoluble melanin pigment leaking from dying melanoma cells represented a target for radioimmunoscintigraphy in a murine xenograft model using a melanin-specific mAb (24), and may be useful for radioimmunotherapy.

Overall, there is an unmet need for a robust and accurate method to detect tumor responses to antineoplastic treatments. Early identification of treatment response would permit continuation of useful treatment and discontinuation of futile treatment so that alternative or experimental treatments may be instituted. We have discovered a new class of cell death antigens, which are malignancy-associated ribonucleoproteins induced in tumor cells because of a DNA damage response. In our previous studies, we described a new cell death ligand, the anti-La ribonucleoprotein mAb 3B9, as a specific malignancy-related marker for chemotherapy-induced apoptosis (Al-Ejeh et al., preceding article). We now describe the specific accumulation of 3B9 in a syngeneic thymic lymphoblastic lymphoma model after chemotherapy. To show *in vivo* targeting of La-specific mAb, we used the EL4 lymphoma model in which apoptosis is induced using cytotoxic chemotherapy. A pattern of "DNA laddering" in tumor cells confirmed apoptotic cell death and terminal deoxyribonucleotide transferase–mediated nick-end labeling–positive dead cells were distributed heterogeneously in s.c. tumors (25). Our data show proof-of-principle for efficient targeting of dead malignant cells in tumors after chemotherapy, which we propose will be required to initiate "cycles of death" and so enhance tumor-directed cytotoxicity of combining chemotherapy with radioimmunotherapy.

Materials and Methods

Cell culture and mAb production. The EL4 murine T-lymphoblastic lymphoma cell line was obtained from American Type Cell Culture (TIB-39) and murine thymocytes were freshly prepared from 6- to 8-week-old C57BL/6 mice. Cells were cultured in RPMI 1640 containing 5% FCS (JRH Biosciences, Inc.) and passaged every 48 to 72 h at a 1:4 dilution. 3B9 and its Sal5 isotype control were prepared as described (Al-Ejeh et al., preceding article). FITC conjugation of these reagents was done according to the manufacturer's instructions (Sigma-Aldrich Co.).

Induction of cell death. Cell death in cultures was induced by adding 20 μg/mL cyclophosphamide (Bristol-Myers Squibb Company, Princeton, NJ) and 20 μg/mL etoposide (Pfizer, Inc.). Cell viability determined by propidium iodide or trypan blue staining was ≥90%

among control untreated cells (data not shown). Viable cells were fixed and permeabilized by incubating cells at 5×10^6/mL in 2% w/v paraformaldehyde solution in PBS [150 mmol/L sodium phosphate and 150 mmol/L sodium chloride (pH 7.2)] for 10 min followed by 1:10 dilution in absolute methanol (at -20°C) for 1 to 3 min before a final wash with PBS.

Flow cytometry, SDS-PAGE, and immunoblotting. Immunofluorescence staining, cytofluorographic analysis, SDS-PAGE, and immunoblotting were done as described (Al-Ejeh et al., preceding article).

Radioligand binding studies. 3B9 and Sal5 control mAb were biosynthetically labeled with ^{14}C using a miniPERM bioreactor (Vivascience GmbH) as described (26). Antibodies in medium from the production chamber were affinity-purified using protein G columns. Radioactivity of purified antibodies (10 μL sample) was counted in UltimaGold scintillation liquid (1 mL) for 20 min using a Packard Tri-Carb 3100 β-counter (Perkin-Elmer, Inc.), which was regularly calibrated using the supplied ^{14}C standards. Protein concentrations were determined using the BCA protein assay. The specific radioactivity values of ^{14}C-Sal5 control and [14]C-3B9 mAb were 120.3 and 130.8 dpm/μg, respectively. Saturation binding was done by incubating dead EL4 cells (5×10^5), which had been treated for 48 h with 20 μg/mL cyclophosphamide and 20 μg/mL etoposide, with increasing concentrations of [14]C-3B9 in the presence (to measure nonspecific binding) or absence (to measure total binding) of a 50-fold molar excess of unlabeled 3B9. After 30 min, cells were washed thoroughly using PBS and β-counts were measured. Specific binding was calculated as the difference between total and nonspecific binding and plotted as a function of [14]C-3B9 concentration. Competition binding assays were carried out by incubating dead EL4 cells with 100 nmol/L [14]C-3B9 in the presence of increasing concentrations of unlabeled 3B9. Then, β-counts were measured and plotted as function of unlabeled 3B9 concentration. Association assays were done by incubating dead EL4 cells with 100 nmol/L [14]C-3B9 in the presence or absence of a 50-fold molar excess of unlabeled 3B9 for the specified times. Samples were washed, radioactivity was measured, and specific binding was plotted as function of time. Dissociation assays were done after incubation of dead EL4 cells with 100 nmol/L [14]C-3B9 in the presence or absence of a 50-fold molar excess of unlabeled 3B9 for 30 min at room temperature. Cells were washed, incubated at 37°C in PBS, and samples were removed at the specified times. Samples were washed with PBS, radioactivity was measured, and specific binding was plotted as function of time.

EL4 tumor model in C57BL/6 mice. The well-characterized EL4 lymphoma model of apoptosis induction was used (25). Subcutaneous EL4 tumor implants were established in 6- to 8-week-old syngeneic C57BL/6 mice by s.c. inoculation of 10^6 EL4 cells in the right flank. Mice were housed and treated as per protocols approved by the Animal Ethics Committees at The University of Adelaide and at the Institute of Medical and Veterinary Sciences. Once tumors reached 1-cm diameter, mice were divided randomly into control or treatment groups.

Treatment comprised i.p. injections of cytotoxic chemotherapy given in one of the following five regimens of escalating dose intensity. For each regimen, the corresponding cyclophosphamide and etoposide doses are indicated (mg/kg). (*a*) quarter dose 1 day: 25, 19 at 0 h; (*b*) quarter dose 2 days: 25, 19 at 0 and 24 h; (*c*) half dose 1 day: 50, 38 at 0 h; (*d*) half dose 2 days: 50, 38 at 0 and 24 h; (*e*) full dose as published (25): 100, 76 at 0 and 24 h.

Cytofluorographic analysis of control and treated EL4 tumors. Control and treated mice bearing EL4 tumors were euthanized 48 h after treatment and tumors were excised. Excised tumor tissue was disrupted by incubation in RPMI 1640 containing 2 mg/mL collagenase type II (Sigma-Aldrich) for 30 min at 37°C with constant shaking. Single-cell suspensions were washed with PBS and used for immunofluorescence staining with 3B9-FITC or Sal-FITC and propidium iodide and flow cytometry analysis as described above.

[14]C-3B9 biodistribution in EL4 tumor-bearing mice. Control and treated EL4 tumor-bearing mice received i.v. injections of [14]C-3B9 or

Fig. 1. La-specific mAb binds specifically to malignant EL4 cells after *in vitro* treatment with cytotoxic drugs. EL4 cells were cultured for 48 h in the absence (*A* and *B*) or presence (*C*) of cyclophosphamide and etoposide. Untreated control cells (*A*), fixed and permeabilized cells (*B*), and cytotoxic drug-treated cells (*C*) were stained with 7-AAD and Sal5 isotype control or La-specific 3B9 mAb. Density plots show fluorescence from Alexa488 (*X axis*) and 7-AAD (*Y axis*). *D,* EL4 cells and syngeneic murine thymocytes (*Thymo.*) were fixed and permeabilized (*clear columns*) or cultured for 48 h with cyclophosphamide and etoposide and subsequently treated (*striped columns*) or not (*filled columns*) with Triton X-100. Columns, 3B9-specific binding presented as net median fluorescence intensity (*MFI*) (*n* = 3) of 7-AAD+ events; bars, SE. ***, *P* < 0.001. Inset, immunoblots of cell lysates were probed for expression of La using 3B9.
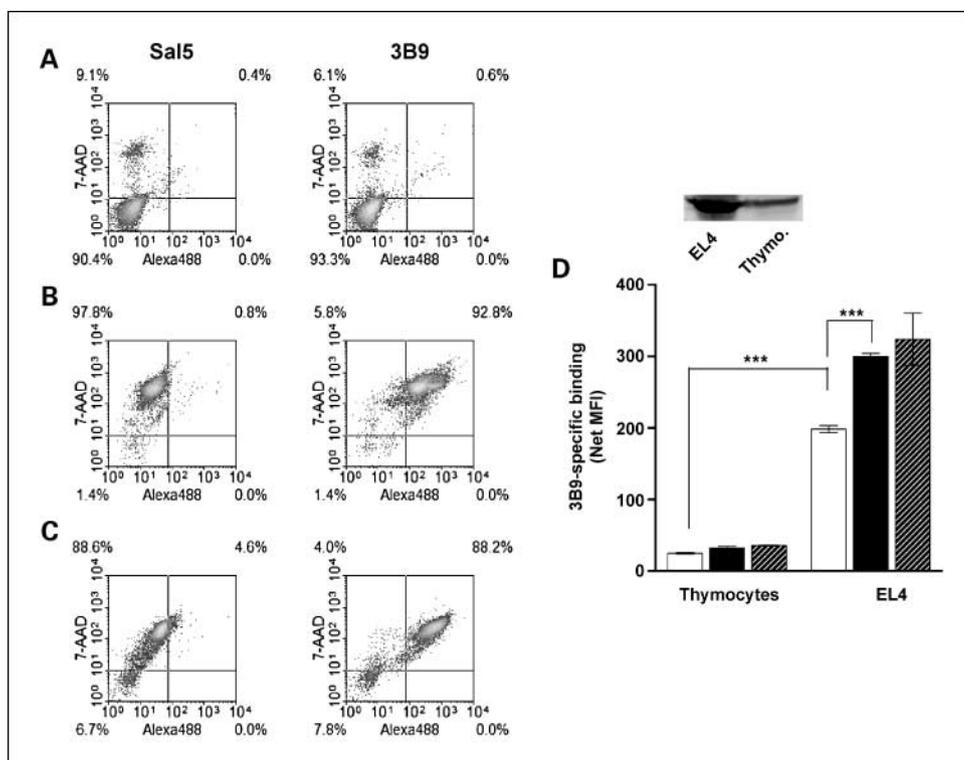
[14]C-Sal5 (isotype control) at 0 h. After 48 h, mice were euthanized, whole blood was collected by cardiac puncture, and EL4 tumors and other tissues were collected for radioactivity measurements. Sera and body tissues were solubilized using 1 mL Solvable (Perkin-Elmer) for 2 h at 50°C, and then decolorized using 100 μL H_2O_2 (30%; Sigma-Aldrich). UltimaGold scintillation liquid (1 mL) was added and samples were counted for 10 min using the β-counter.

[111]*In–1,4,7,10-tetra-azacylododecane-N,N′,N″,N″′-tetraacetic acid–3B9 biodistribution and pharmacokinetics in EL4 tumor-bearing mice.* Protein G–purified 3B9 or Sal5 mAb were mixed at 2.5 mg/mL in 0.1 mol/L sodium bicarbonate and 0.1 mol/L sodium phosphate buffer (pH8.5) with a 50-fold molar excess of 1,4,7,10-tetra-azacylododecane-N,N′,N″,N″′-tetraacetic acid mono-(N-hydroxysuccinimidyl) ester (DOTA-NHS-ester; Macrocyclics) dissolved in DMSO (Sigma-Aldrich). DMSO represented <10% of the final reaction, which was incubated for 2 h at 23°C with constant vigorous shaking. DOTA-NHS-ester was added at a 50-fold molar excess to the antibody as this ratio was found to minimize inactivation of 3B9 and showed favorable *in vivo* biodistribution compared with either Sal5 conjugated at the same ratio or 3B9 conjugated at higher ratios (data not shown). Addition of 1.5 mol/L Tris-HCl (pH 8.8) at a final dilution of 1:10 was used to stop the reaction. Reactions were purified and buffer-exchanged into PBS using 100-kDa cutoff microconcentrators as per the manufacturer's instructions (Millipore). F(ab)2 fragments of DOTA-conjugated 3B9 were prepared by pepsin digestion where 10 mg of DOTA-conjugated 3B9 (prepared as above) was incubated (2 h at room temperature) with 1 mg of pepsin-agarose beads (Sigma-Aldrich Co.) in a final 1 mL volume of 100 mmol/L sodium acetate buffer (pH 4). The reaction was neutralized with 1.5 mol/L Tris-HCl (pH 8.8); the agarose beads were removed by centrifugation; and the supernatant was purified using Protein A columns (Amersham Biosciences) to remove undigested IgG. The reaction was further purified and buffer exchanged into PBS using a 50-kDa cutoff microconcentrator as per the manufacturer's instructions (Millipore) to remove Fc fragments. The concentrations of 3B9-DOTA and the F(ab)2 fragments of 3B9-DOTA were measured using a BCA protein assay kit and the concentration of conjugated DOTA was measured using a modification (27) of a

published Cu:Arsenazo(III) assay (28–30). The ligand/protein (L/P) ratio of 7.5 or 5.1 was calculated as the ratio of the concentrations (μmol/L) of DOTA in the immunoconjugates to 3B9 or F(ab)2 fragment of 3B9 (μmol/L), respectively. Immunoconjugates were stored at 4°C before radiolabeling.

Purified DOTA immunoconjugates were radiolabeled with indium-111 (^{111}In; Perkin-Elmer) as described (31–36). Radiolabeled immunoconjugates were purified using 100- or 50-kDa cutoff microconcentrators for IgG or F(ab)2 fragment, respectively, according to the manufacturer's instructions. The incorporation of ^{111}In in the purified reaction products was determined using instant TLC, which was done using instant TLC-SG strips (Pall Corp.) as described (31–36). Although 99% of radioactivity on the instant TLC-SG strip was at the solvent front when instant TLC was done using [111]InCl3 solution, 99% of radioactivity in the DOTA immunoconjugates remained at the origin, indicating the complete incorporation of ^{111}In in the DOTA conjugates (data not shown). At 0 h, ^{111}In-DOTA immunoconjugates (~75 μg in 100 μL of PBS) were given by i.v. injection to EL4 tumor-bearing mice, which were left untreated or treated with cytotoxic chemotherapy as described above. Mice were euthanized at selected time points, blood was collected by cardiac puncture, and tumors and organs were harvested. Blood and organs were weighed and placed in gamma counter tubes, and radioactivity was measured using the Cobra 5010 gamma counter (Perkin-Elmer) normalized for ^{111}In counting using a 100 to 350 keV counting window. Radioactivity in organs was normalized to the weight of the organs and accumulation was calculated as the percentage of radioactivity per gram in the organs over the radioactivity of the injected dose of ^{111}In-DOTA immunoconjugates at 0 h (%ID/g). Time-activity curves for blood and tumors were constructed using GraphPad Prism v.4 (GraphPad Software) for each treatment group where accumulation %ID/g (±SE, *n* = 5) was plotted as a function of time. Curves were fitted to one-phase exponential decay for blood, and one-phase exponential association for tumors and half-life ($t_{1/2}$) values are provided from the fitted models. In the case of tumor accumulation, the fitted association model also provided a value for maximal accumulation at saturation together with the corresponding SE of this measurement, which we report as

%ID/g $\pm$ SE at saturation. Data points did not deviate from the fitted models, which was evaluated by a runs test done using the fitting software. Regression values of the fitted model are provided.

Statistical analysis. Statistical comparisons were done using Graph-Pad Prism v4. Two-way ANOVA was used to deduce significant differences among the results. The Bonferroni posttest comparison was used to report P values. P values are denoted as follows: *, $P < 0.05$; **, $P < 0.01$; ***, $P < 0.001$.

Results

La is overexpressed in malignant EL4 cells, and La-specific mAb binding to dead EL4 cells is induced by DNA-damaging drugs. Although 5% to 10% of EL4 cells bound 7-amino-actinomycin (7-AAD) as evidence of spontaneous cell death in culture, <1% bound La-specific mAb 3B9 (Fig. 1A). However, 3B9 bound nearly all fixed and permeabilized 7AAD+ EL4 cells, indicating that La could be accessed with specific mAb (Fig. 1B). After treatment with cyclophosphamide and etoposide, the binding of 3B9 to 7-AAD+ EL4 cells was even more intense (Fig. 1C) and was quantified as per cell binding (Fig. 1D). Moreover, 3B9 still bound EL4 cells killed with cytotoxic drugs after treatment with nonionic detergent, which suggested that La was cross-linked in dead cells (ref. 37; Fig. 1D). Figure 1D also illustrates that, after fixation and permeabilization, per cell binding of 3B9 was significantly higher for the malignant EL4 cell than for its counterpart primary cell type of the thymocyte and this result was corroborated by immunoblot analysis of cell lysates (Fig. 1D, *inset*). Importantly, 3B9 binding to dead thymocytes was similar irrespective of the mode of cell death, whereas 3B9 binding to dead EL4 cells killed by cytotoxic drugs was significantly greater (Fig. 1D).

14C-labeled 3B9 binds specifically to EL4 cells. We used intrinsically labeled 3B9 mAb to characterize further binding of La-specific mAb to EL4 cells killed by cytotoxic drugs. The concentration of ^{14}C-3B9 at half-maximal saturation was 18 nmol/L, maximal binding was ~ 7,500 fmol per 10^6 dead cells (Fig. 2A), and half-maximal saturation of ^{14}C-3B9 binding occurred within 5 min (Fig. 2B). The concentration of unlabeled 3B9 required to inhibit half-maximal binding of ^{14}C-3B9 (IC_{50}) was 118 nmol/L (Fig. 2C), and minimal dissociation of bound 3B9 occurred (Fig. 2D). Altogether, these data describe specific, rapid, saturable, and high-avidity binding of ^{14}C-3B9 to dead tumor cells. No EL4 binding was detected without cytotoxic drug treatment (data not shown), which indicated that binding depended on induction of cell death.

Cytotoxic chemotherapy increases the target for 3B9 in the tumor mass. Next, we used the EL4 lymphoma model to ascertain if the *in vitro* findings pertained *in vivo*. After chemotherapy, the fraction of propidium iodide–positive cells in tumor explants increased significantly from a mean ($\pm$SE) of 50 $\pm$ 2% to 70 $\pm$ 1% ($P < 0.001$). Similarly, the 3B9+ subset of propidium iodide–positive cells increased significantly from 15 $\pm$ 1% to 38 $\pm$ 2% ($P < 0.01$) after chemotherapy, whereas isotype control staining was unaltered (Fig. 3). Only the propidium iodide–positive tumor subpopulation bound 3B9, which indicated that La was recognized specifically in dead tumor cells. Histogram analysis (Fig. 3) indicated that specific per cell binding of 3B9-FITC to propidium iodide–positive cells was significantly augmented in tumors exposed *in vivo* to cytotoxic chemotherapy (net median fluorescence intensity $\pm$ SE of 18 $\pm$ 3 with chemotherapy and 1 $\pm$ 3 without chemotherapy, $P < 0.05$).
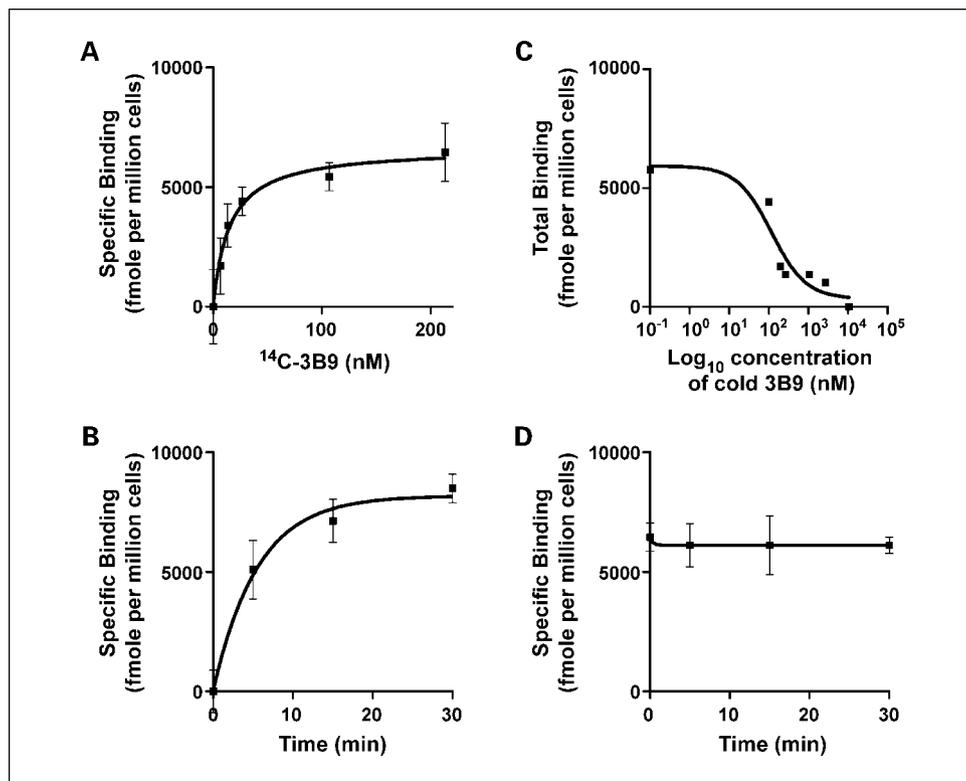

Fig. 2. ^{14}C-3B9 mAb binds with high avidity to dead EL4 cells in a specific, rapid, and saturable manner. EL4 cells were killed with cyclophosphamide and etoposide. *A,* treated cells were incubated with increasing concentrations of ^{14}C-3B9 in the presence or absence of a 50-fold molar excess of unlabeled 3B9. Specific binding was calculated in units of femtomole bound per 10^6 cells and plotted as a function of ^{14}C-3B9 concentration ($n = 3$; $r^2 = 0.99$). *B,* dead EL4 cells were incubated with ^{14}C-3B9 and samples were removed for analysis at specified time points. Specific binding in units of femtomole bound per 10^6 cells was plotted as a function of time ($n = 3$; $r^2 = 0.90$). *C,* apoptotic EL4 cells were incubated with 100 nmol/L ^{14}C-3B9 in the presence of increasing concentrations of unlabeled 3B9. Radioactivity was measured and converted to units of femtomole bound per 10^6 cells and plotted as a function of the log concentration of 3B9 ($n = 5$; $r^2 = 0.85$). *D,* apoptotic EL4 cells were incubated with ^{14}C-3B9 for 30 min. Cells were washed and then incubated in binding buffer alone, and samples were removed at specified time points. Specific binding in units of femtomole bound per 10^6 cells was plotted as a function of time ($n = 3$; $r^2 = 0.90$).

Fig. 3. La-specific 3B9 mAb binds specifically to dead EL4 tumor explant cells, particularly after induction of La by cytotoxic drug treatment of EL4 tumor-bearing mice. EL4 tumor-bearing mice (*n* = 5) were treated or not with cyclophosphamide and etoposide, and after 48 h excised tumor cells were stained with 3B9 or its isotype control Sal5 mAb and propidium iodide (*PI*). Data are representative density plots and histogram overlays of FITC and propidium iodide fluorescence emissions from stained cells, which were isolated from EL4 tumor explants of mice treated (+; *bottom row*) or not (-; *top row*) with cytotoxic chemotherapy. Data depicted in the histogram overlays originated from region 1 (*R1*), which represents the FITC – positive subset of propidium iodide – positive events, and shows Sal5-FITC staining of tumor cells from treated mice (*gray fill*) and 3B9-FITC staining of tumor cells from untreated mice (*dashed line*) and treated mice (*thick line*).
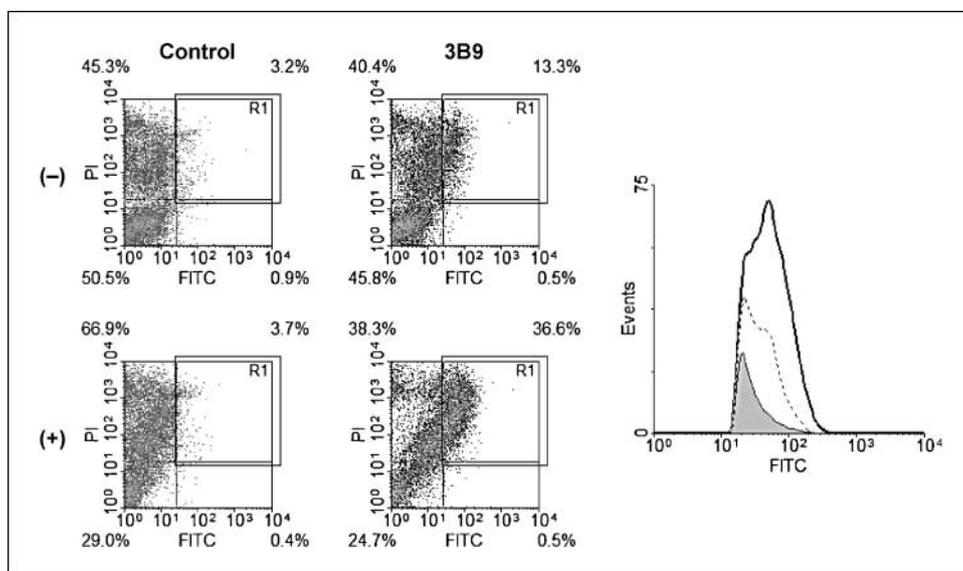
3B9 targets EL4 tumors **in vivo** *especially after cytotoxic chemotherapy.* We studied the biodistribution of La-specific mAb in the EL4 lymphoma model using intrinsically or extrinsically labeled 3B9 mAb. EL4 tumor-bearing mice (*n* = 4-5) were treated with full-dose chemotherapy and simultaneously given 100 μg of ^{14}C-3B9 or ^{14}C-Sal5 isotype control mAb and analyzed 48 h later. The ^{14}C-Sal5 mAb did not accumulate significantly in any organ or tissue, including the tumor. In contrast and compared with all other organs, ^{14}C-3B9 accumulated significantly in both serum and tumor (*P* < 0.001). Without chemotherapy, %ID/g (±SE) in tumor was 14.7 ± 1.2% and 1.1 ± 0.2% for ^{14}C-3B9 and ^{14}C-Sal5, respectively. Moreover, after chemotherapy, only tumors accumulated significantly more ^{14}C-3B9 (*P* < 0.001). With chemotherapy, %ID/g (±SE) in tumor was 25.9 ± 5.1% and 1.7 ± 0.4% for ^{14}C-3B9 and ^{14}C-Sal5, respectively. The accumulation of ^{14}C-3B9 mAb in normal tissues was unaltered by chemotherapy. The %ID/g (±SE) values for normal tissues of control untreated mice versus treated mice were as follows: 6.0 ± 0.3 versus 5.2 ± 0.7 (spleen), 4.3 ± 0.5 versus 3.2 ± 0.2 (kidneys), 6 ± 3 versus 7 ± 3 (liver), and 17 ± 3 versus 17 ± 2 (blood). These data indicated that tumor accumulation of 3B9 mAb was an inherent property of its antigen-binding activity.

In the second series of experiments, the biodistribution and pharmacokinetics of ^{111}In-labeled and DOTA-conjugated 3B9 was investigated in EL4 tumor-bearing mice with and without chemotherapy (Figs. 4 and 5). Blood clearance of ^{111}In-DOTA-3B9 in untreated control mice and in mice treated with half dose 1-day or quarter dose 2-day regimens was not significantly different (*P* > 0.05). On the other hand, blood clearance of ^{111}In-DOTA-3B9 in mice treated with half dose 2-day or quarter dose 1-day regimens was significantly faster than in control mice (*P* < 0.001; Fig. 4). As predicted by curve-fitting models, maximal tumor accumulation of ^{111}In-DOTA-3B9 in mice treated with either the half dose 1-day (40 ± 3%ID/g; *n* = 5) or quarter dose 2-day (37 ± 3%ID/g; *n* = 5) regimens was significantly different from that in control mice (20 ± 1%ID/g; *n* = 5; *P* < 0.05). The more rapid clearance of ^{111}In-DOTA-3B9 from blood of mice treated with the half dose 2-day and quarter dose 1-day regimens was associated with significantly greater

tumor accumulation (48 ± 8%ID/g; *n* = 5 and 47 ± 6%ID/g; *n* = 5, respectively; *P* < 0.01; Fig. 4). Despite the exponential growth of control tumors (Fig. 4), weight-normalized tumor accumulation (%ID/g) of ^{111}In-DOTA-3B9, which has a physical half-life of 2.8 days, was unchanged, which suggested that rates of tumor cell death balanced tumor cell proliferation so that 3B9 continued to bind these growing tumors. The dose intensity of cytotoxic chemotherapy was directly related to the extent of tumor shrinkage and to the extent of tumor cell death recorded as %7-AAD$^+$ cells (Fig. 4, *inset*). In mice treated with the half dose 2-day regimen, the linear increase in tumor content of apoptotic cells at 48 and 72 h postinjection correlated with the linear increase in tumor accumulation of radioactivity. For other chemotherapy regimens, insufficient data prevented a clear relationship between extent of tumor cell death and tumor radioactivity accumulation being determined, although both tumor cell death and accumulation were greater for half dose 1-day and quarter dose 2-day regimens than for control (Fig. 4).

The specificity of 3B9 for dying tumors was determined from the ratio of radioactivity accumulation in tumor to that in normal organs (tumor/organ ratio; Fig. 5). All tumor/organ ratios for treated mice (except for tumor/blood ratio) were significantly greater than for control mice 48 h (Fig. 5A) and 72 h (Fig. 5B) postinjection although the tumor/blood ratio did exceed unity at 72 h only. In contrast, tumor/blood ratios exceeding unity were obtained at both 48 h (Fig. 5C) and 72 h (Fig. 5D) after administration of F(ab)$_2$ fragments of 3B9. Improved tumor/blood ratios resulted primarily from very rapid blood clearance of F(ab)$_2$ fragments with half-lives ($t_{1/2}$; ±SE) of 10.3 ± 0.1, 8.6 ± 0.1, 8.6 ± 0.1, 10.2 ± 0.1, and 7.8 ± 0.1 h for control untreated mice, and mice treated with carboplatin and etoposide according to the half dose 2-day, half dose 1-day, quarter dose 2-day, and quarter dose 1-day regimens, respectively. Consistent with the rapid blood clearance rates, tumor accumulation rates of F(ab)$_2$ fragments of 3B9 also increased where the accumulation half-lives ($t_{1/2}$; ±SE) for the half dose 2-day, half dose 1-day, quarter dose 2-day, and quarter dose 1-day regimens were 1.4 ± 0.2, 1.7 ± 0.2, 2.4 ± 0.2, and 2.7 ± 0.3 h, respectively.

Further evidence for tumor specificity was obtained from biodistribution studies of ^{14}C-3B9 in EL4 tumor-bearing mice, which were extended to include lower doses of the radio-labeled agent. No significant accumulation of ^{14}C-3B9 occurred in any tissue except the tumor and only after administration of cytotoxic chemotherapy. Tumor accumulation of ^{14}C-3B9 was dose dependent and the sigmoidal dose-response relationship suggested that target binding was specific and saturable (Fig. 6). In comparison with untreated mice, tumor uptake of ^{14}C-3B9 with chemotherapy was significantly higher and showed fold increases of 1.9, 1.9, and 1.8 at ^{14}C-3B9 doses of 25, 50, and 100 μg, respectively. Altogether, using two different radiotracer formats, we showed specific and preferential tumor accumulation of 3B9, which was markedly augmented by cytotoxic chemotherapy in this chemoresponsive tumor model.

Discussion

The use of radiolabeled mAb to identify necrotic cells *in vivo* was first reported as a means of identifying myocardial infarction (38, 39). Epstein et al. (20, 40) selected a tumor necrosis therapy series of mAb that preferentially recognized insoluble nuclear antigens in necrotic and degenerating areas of tumors. Of the series, TNT1, TNT2, and TNT3 mAbs recognize the universal nuclear antigens histone 1, histone 2, and histone 3 (21), and ssDNA (41), respectively. These mAb reagents are intended to target necrotic regions in solid tumors for the purposes of diagnosis, staging, and radioimmunotherapy of cancer (42). Now, we describe a promising new nuclear target antigen, which has characteristics differentiating it from previously described targets and which we hypothesize will increase its utility as a dead cell target antigen for radio-immunoscintigraphy and radioimmunotherapy.

We found that the La autoantigen was overexpressed in malignancy both at mRNA and protein levels. DNA-damaging drugs augmented specific binding of 3B9 to dead human cancer cells *in vitro* when its binding correlated with the extent of an early DNA-damage response. These data suggested that La might be involved in early DNA-damage response mechanisms. Later, concurrent with the onset of apoptosis, La became fixed in apoptotic cells because of TG2-mediated protein cross-linking and 3B9 accumulated in various human cancer cell lines in a time-dependent, specific, and saturable manner.
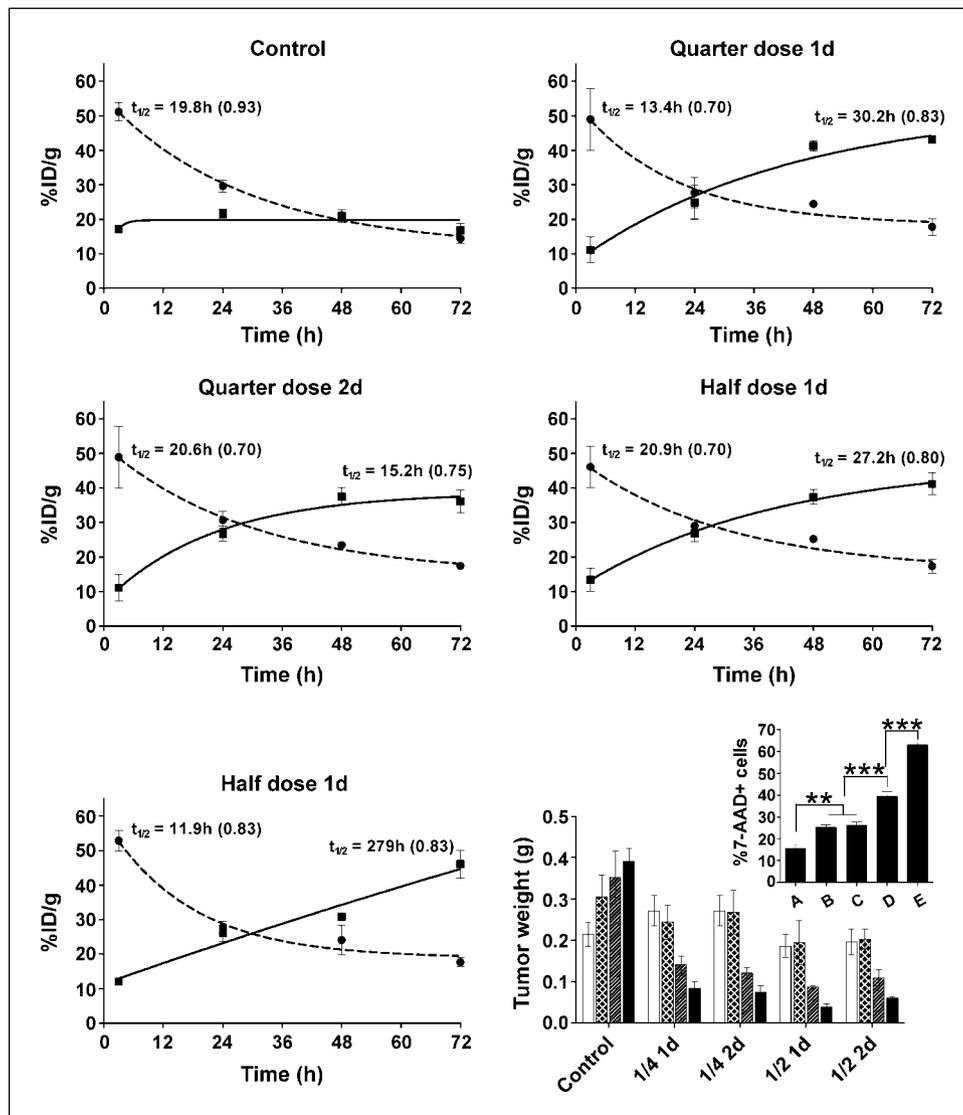

Fig. 4. Time-activity curves of ^{111}In-DOTA-3B9 in EL-4 tumor-bearing mice treated or not with cytotoxic chemotherapy. EL4 tumor-bearing mice ($n = 5$) were left untreated (*Control*) or treated with cyclophosphamide and etoposide using four different regimens of escalating dose intensity. For each analysis time point after ^{111}In-DOTA-3B9 administration, data are expressed as percentage of organ radioactivity normalized to organ weight and divided by radioactivity of injected dose (%ID/g). Points, mean; bars, SE. Time-activity curves were fitted for blood (- - -) and tumor (—). Half-life ($t_{1/2}$) values for blood clearance and tumor accumulation are displayed next to each fitted curve and regression values are shown in brackets. Bottom right, graph showing tumor weights (g) from control and treated mice. Columns, mean measured at 3 h (*clear*), 24 h (*hatched*), 48 h (*striped*), and 72 h (*filled*) postinjection; bars, SE. Inset, in separate experiments, single-cell suspensions prepared from EL4 tumors ($n = 4$) were analyzed by flow cytometry for 7-AAD binding at 48 h postinjection for untreated mice (*A*) or mice treated with the following chemotherapy regimens: quarter dose 2 d (*B*), half dose 1 d (*C*), half dose 2 d (*D*), and half dose 2 d analyzed at 72 h postinjection (*E*). Columns, mean of %7-AAD$^+$ tumor cells; bars, SE. Statistical comparisons were made as indicated: **, $P < 0.01$; ***, $P < 0.001$.

Fig. 5. Tumor-targeting efficiency of ^{111}In-DOTA-3B9 and ^{111}In-DOTA-F(ab)$_2$ fragments of 3B9 is enhanced by cytotoxic chemotherapy. Accumulation of ^{111}In-DOTA-3B9 in tumor (%ID/g) was measured at 48 h (*A*) and 72 h (*B*) postinjection and divided by accumulation in other organs at specified time points. Similarly, the accumulation of ^{111}In-DOTA-F(ab)$_2$ 3B9 in tumor (%ID/g) at 48 h (*C*) and 72 h (*D*) was divided by accumulation in other organs at these time points. Columns, mean tumor/organ ratios for control mice (*clear*), mice treated with quarter dose 1 d (*filled*), quarter dose 2 d (*striped*), half dose 1 d (*hatched*), or half dose 2 d (*stippled*); bars, SE. Solid line, a tumor/organ ratio of 1. Statistical comparisons were made with control mice: **, *P* < 0.01; ***, *P* < 0.001. It should be noted that tumor/kidney ratios for ^{111}In-DOTA-F(ab)$_2$ 3B9 were significantly less than 1, which was attributed to high renal reuptake of F(ab)$_2$ or Fab fragments.
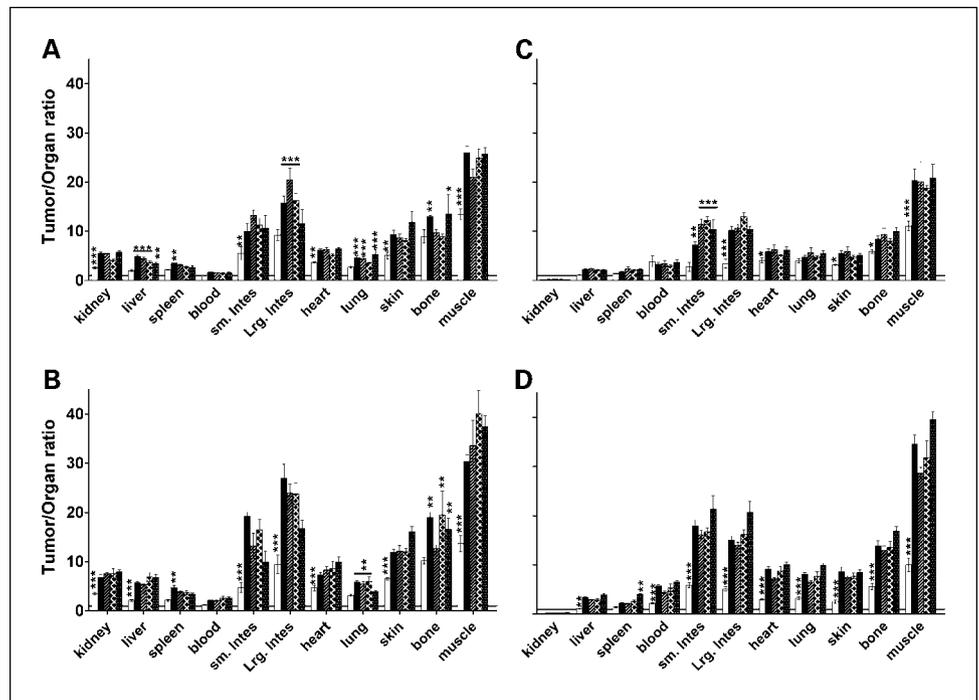
Moreover, protein cross-linking in dead malignant cells extended to include fixation of La-bound 3B9 so that its levels were higher than in dead primary cells (Al-Ejeh et al., preceding article). Based on these *in vitro* findings, we hypothesized that 3B9 would be a useful cancer-specific cell death ligand for the detection and targeting of dead tumor cells *in vivo*, particularly after induction of tumor cell death by DNA-damaging agents.

Here, we provide *in vivo* proof-of-principle for the ability of 3B9 to target dead and dying tumor cells after DNA-damaging chemotherapy. We adopted a murine tumor model of robust apoptosis induction with use of DNA-damaging agents (25) to investigate the binding characteristics of 3B9 *in vivo*. Results of initial *in vitro* studies using the EL4 lymphoma cell line supported earlier *in vitro* findings using human cancer cell lines (Al-Ejeh et al., preceding article). La-specific mAb 3B9 bound dead EL4 cells more avidly than dead thymocytes. Binding of 3B9 was induced after EL4 cells were treated with DNA-damaging agents and the binding was preserved despite treatment of the dead EL4 cells with a nonionic detergent, which indicated that the La target antigen was cross-linked in dead EL4 cells. Using a ^{14}C-labeled form of the mAb, 3B9 binding to dead EL4 cells was shown to be specific, rapid, saturable, and of high avidity. EL4 tumors removed from treated mice exhibited excessive cell death in comparison with tumors derived from untreated mice. *Ex vivo* staining of these dead tumor cells showed that not only did a higher proportion of dead tumor cells obtained from treated mice bind 3B9, but that the per cell binding of 3B9 was significantly higher among dead tumor cells derived from treated mice than from untreated control mice.

Based on these *in vitro* data and on the tumor explant data, we chose the EL4 tumor model to investigate the performance of 3B9 *in vivo*. Using two different radiotracer formats, [14]C-3B9 and ^{111}In-DOTA-3B9, we report specific and saturable binding of 3B9 in EL4 tumors *in vivo* after chemotherapy. In untreated

mice, 3B9 accumulation was stable during exponential tumor growth, which we attributed to the ability of 3B9 to bind dead cells present endogenously in these tumors. In contrast, cytotoxic chemotherapy, which reduced tumor mass and increased tumor cell death, significantly augmented tumor accumulation of 3B9 48 h or more after chemotherapy. Although we cannot formally exclude the possibility that there was postchemotherapy release of La antigen from secondarily necrotic tumor cells into the circulation, we believe that insufficient La antigen was released to alter blood clearance rates of radiolabeled 3B9 mAb because, as illustrated in Fig. 4, these rates were similar irrespective of the use of chemotherapy.

Hence, we hypothesize that DNA-damaging agents induced La to the extent that its binding levels among "murdered" tumor cells were greater than among tumor cells dying from "neglect." In support, our *in vitro* data showed that 3B9 binding was significantly less in malignant cells dying from serum withdrawal than in malignant cells dying after DNA-damaging cytotoxic drug treatment (Al-Ejeh et al., preceding article). Similarly, treatment of Jurkat cells *in vitro* with other primary necrotic stimuli such as heat (56°C for 1 h), 0.1% H_2O_2, 5% ethanol, 0.1% $HgCl_2$, and 1% sodium azide followed by 48 h in culture produced lower 3B9-specific binding than the binding observed after fixation and permeabilization of the Jurkat cells using paraformaldehyde and methanol. Importantly, all 3B9 binding to primary necrotic cells at 48 h postinduction was significantly lower than 3B9 binding 48 h after treatment of Jurkat cells with the DNA-damaging drug, cisplatin (Al-Ejeh et al., preceding article).

In addition, we did studies of activated caspase-3 as a marker of apoptosis in EL4 tumors treated or not with carboplatin and etoposide chemotherapy. We found that the increased tumor accumulation of ^{111}In-DOTA-3B9 after carboplatin and etoposide chemotherapy correlated with the postchemotherapy apoptotic index, which was measured using quantitative video

image analysis as the ratio of the proportion of apoptotic cells expressing activated caspase-3 to the proportion of viable tumor cells. Using the same form of analysis of H&E–stained sections; we found that the centrally necrotic areas in control untreated tumors extended as the tumors grew in size. In contrast, as the apoptotic index increased in tumors of carboplatin and etoposide–treated mice, the necrotic areas identified by H&E shrank in proportion to the overall shrinkage of tumor size. None of these necrotic areas in control untreated or treated tumors stained for activated caspase-3.[4] Hence, we propose that the mode of cell death determines the extent of 3B9 binding. In contrast to primary necrosis, chemotherapy-induced apoptosis is associated with DNA damage responses, which, in conjunction with other early apoptotic signaling, induces TG2 to cross-link the overexpressed La target antigen. Therefore, whereas a multitude of dead cell target antigens would be available for binding in areas of endogenous tumor necrosis, we argue that the generation of apoptotic tumor cells in response to DNA-damaging antineoplastic therapy would increase the availability of only a subset of target antigens such as La and other ribonucleoproteins. We envisage a two-step targeting process in which DNA-damaging antineoplastic therapy first creates overexpressed and cross-linked targets that can subsequently be bound by radiolabeled antibodies to enhance the tumor/background ratio for imaging applications or the therapeutic ratio for therapeutic applications. It is this chemotherapy-induced 3B9-binding effect that we believe represents an important point of difference from other methods that localize mAb binding in regions of tumor cell death (20, 24).

Milas et al. (43) observed that the cytotoxic radiosensitizing drug, gemcitabine, induced apoptosis in jejunal crypt cells, which resolved by 24 to 36 h posttreatment. We showed that both tumor cell death measured by *ex vivo* 7-AAD staining of tumor explant cells and tumor uptake of ^{111}In-DOTA-3B9 *in vivo* were evident 24 h after combined administration of chemotherapy and radiotracer and then increased further at later times. Hence, radioimmunoimaging or radioimmunotherapy may need to be scheduled after apoptosis in normal tissues has run its course to avoid La-specific mAb binding to apoptotic normal cells, but before maximal tumor cell death occurs so as to maximize tumor accumulation of radiotracer or radio-dose delivered by La-specific mAb. Such scheduling considerations may also be important if cytotoxic chemotherapy injures vascular endothelium (44) and alters the biodistribution of the mAb and thus its potential for normal tissue toxicity. However, the data we have presented using the Sal5 isotype control antibody suggest that such nonspecific effects have not been significant in this model.

In addition, we investigated the biodistribution of (Fab)$_2$ fragments of ^{111}In-labeled 3B9 in control and treated mice as described herein. The clearance of (Fab)$_2$ from blood was 2- to 3-fold faster than the IgG form of 3B9, whereas augmented accumulation in treated tumors was retained. However, due to its rapid blood clearance, maximum tumor accumulation of ^{111}In-labeled 3B9 (Fab)$_2$ in treated mice was significantly reduced compared with peak accumulation of ^{111}In-labeled 3B9 IgG. Therefore, our results are typical of other studies in which the extended blood pool activity of whole IgG enhances

tumor uptake but reduces tumor/background ratios, whereas the reduced blood pool activity of (Fab)$_2$ reduces tumor uptake but enhances tumor/background ratios (45, 46). Hence, scheduling of the 3B9 injection after chemotherapy and use of F(ab)$_2$ or Fab fragments or Fc-modified versions of whole IgG (42) may improve tumor/background ratios.

Selective *in vivo* targeting of La favors two major applications of this technology in cancer diagnosis and treatment. First, La-directed radioimmunoscintigraphy may detect tumor responses to antineoplastic treatment, in particular, DNA-damaging drugs and ionizing radiation. Second, La-directed radioimmunotherapy would be facilitated by the therapeutic principle of bystander killing, which embraces at least three related concepts. First, ionizing radiation originating from labeled La-specific mAb bound inside dead tumor cells would engender further cytotoxicity in nearby viable tumor cells via radiation crossfire effects. Second, bound radioactivity would exert distant cytotoxic effects via diffusion of radiation-induced second messengers (47). Third, we hypothesize that as radiation-induced killing of tumor cells delivered by labeled La-specific mAb propagates cell death among nearby viable tumor cells, a "virtuous cycle" of tumor cell killing would result as additional targets for binding are created.

After cytotoxic chemotherapy, increased binding of La-specific mAb to EL4 lymphomas depended on brisk and presumably P53-mediated induction of tumor cell apoptosis. However, carcinoma is relatively resistant to conventional cytotoxic chemotherapy and radiotherapy (48). Carcinoma cell death may be slower in onset than previously recognized and comprise nonapoptotic routes to cell death such as necrosis, autophagy, and mitotic catastrophe as well as senescence-like growth arrest
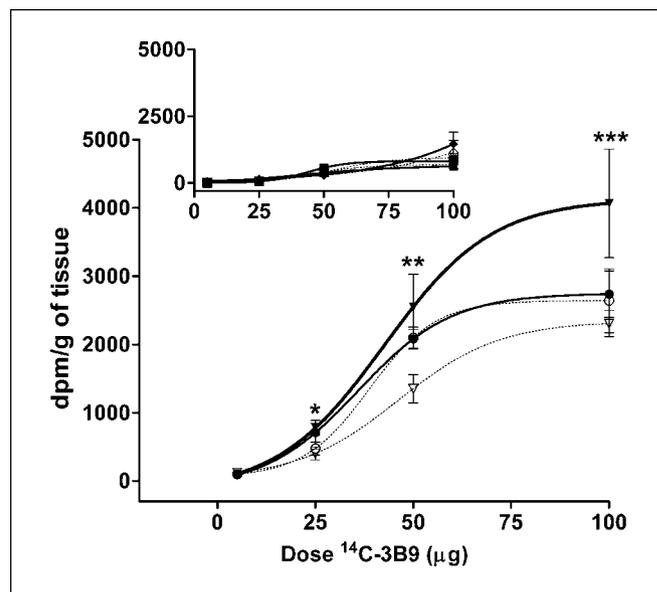

Fig. 6. Tumor accumulation of biosynthetically labeled La-specific [14]C-3B9 mAb is dose dependent and augmented by cytotoxic chemotherapy. The biodistribution of different doses of ^{14}C-labeled 3B9 was studied in EL4 tumor-bearing mice with or without the effects of cytotoxic chemotherapy. EL4 tumor-bearing mice were treated or not with full-dose cyclophosphamide and etoposide and simultaneously administered 5, 25, 50, or 100 µg of [14]C-3B9 or ^{14}C-Sal5. After 48 h, radioactivity measurements were normalized to the mass of tissue counted (dpm/g of tissue) and tissues included liver (◆), spleen (■), kidneys (▲), serum (●), and tumor (▼). Points, dpm/g; bars, SE. Inset, liver, spleen, and kidney values. Closed symbols, with chemotherapy; open symbols, without chemotherapy. Statistical comparisons were made with control mice: *, $P < 0.05$; **, $P < 0.01$; ***, $P < 0.001$.

---

[4] Al-Ejeh et al., manuscript in preparation.

(49). Although these observations may limit the efficiency of our target creation strategy, new classes of compounds are now emerging, which preclinical studies have shown to overcome apoptosis resistance and deliver higher levels of cell death in carcinoma (50). In particular, histone deacetylase inhibitors have promising preclinical activity especially in conjunction with the use of conventional cytotoxic drugs and radiation (51).

In conclusion, we provide proof-of-principle for the specific and preferential accumulation of La-specific mAb in dead tumor cells in which cell death was induced by DNA-damaging agents *in vivo*. Using EL4 and tumor xenograft models, we plan to investigate the utility of our novel tumor targeting strategy for radioimmunoscintigraphy and to test the safety and efficacy of combination chemotherapy and radioimmunotherapy.

References

1. Hanahan D, Weinberg RA. The hallmarks of cancer. Cell 2000;100:57–70.
2. Wyllie AH, Kerr JF, Currie AR. Cell death: the significance of apoptosis. Int Rev Cytol 1980;68:251–306.
3. Symmans WF, Volm MD, Shapiro RL, et al. Paclitaxel-induced apoptosis and mitotic arrest assessed by serial fine-needle aspiration: implications for early prediction of breast cancer response to neoadjuvant treatment. Clin Cancer Res 2000;6:4610–7.
4. Chang J, Ormerod M, Powles TJ, Allred DC, Ashley SE, Dowsett M. Apoptosis and proliferation as predictors of chemotherapy response in patients with breast carcinoma. Cancer 2000;89:2145–52.
5. Davis DW, Buchholz TA, Hess KR, Sahin AA, Valero V, McConkey DJ. Automated quantification of apoptosis after neoadjuvant chemotherapy for breast cancer: early assessment predicts clinical response. Clin Cancer Res 2003;9:955–60.
6. Weber WA. Positron emission tomography as an imaging biomarker. J Clin Oncol 2006;24:3282–92.
7. Lahorte CM, Vanderheyden JL, Steinmetz N, Van de Wiele C, Dierckx RA, Slegers G. Apoptosis-detecting radioligands: current state of the art and future perspectives. Eur J Nucl Med Mol Imaging 2004;31:887–919.
8. Petrovsky A, Schellenberger E, Josephson L, Weissleder R, Bogdanov A, Jr. Near-infrared fluorescent imaging of tumor apoptosis. Cancer Res 2003;63:1936–42.
9. Collingridge DR, Glaser M, Osman S, et al. *In vitro* selectivity, *in vivo* biodistribution and tumour uptake of Annexin V radiolabelled with a positron emitting radioisotope. Br J Cancer 2003;89:1327–33.
10. van de Wiele C, Lahorte C, Vermeersch H, et al. Quantitative tumor apoptosis imaging using technetium-99m-HYNIC Annexin V single photon emission computed tomography. J Clin Oncol 2003;21:3483–7.
11. Blankenberg FG, Katsikis PD, Tait JF, et al. *In vivo* detection and imaging of phosphatidylserine expression during programmed cell death. Proc Natl Acad Sci U S A 1998;95:6349–54.
12. Mochizuki T, Kuge Y, Zhao S, et al. Detection of apoptotic tumor response *in vivo* after a single dose of chemotherapy with ^{99m}Tc-annexin V. J Nucl Med 2003;44:92–7.
13. Belhocine T, Steinmetz N, Hustinx R, et al. Increased uptake of the apoptosis-imaging agent (99m)Tc recombinant human Annexin V in human tumors after one course of chemotherapy as a predictor of tumor response and patient prognosis. Clin Cancer Res 2002;8:2766–74.
14. Jain D, Crawley JC, Lahiri A, Raftery EB. Indium-111-antimyosin images compared with triphenyl tetrazolium chloride staining in a patient six days after myocardial infarction. J Nucl Med 1990;31:231–3.
15. Tamaki N, Yamada T, Matsumori A, et al. Indium-111-antimyosin imaging for detecting different stages of myocardial infarction: comparison with technetium-99m-pyrophosphate imaging. J Nucl Med 1990;31:136–42.
16. Matsumori A, Yamada T, Tamaki N, et al. Persistent uptake of indium-111-antimyosin monoclonal antibody in patients with myocardial infarction. Am Heart J 1990;120:1026–30.
17. Kairemo KJ, Wiklund TA, Liewendahl K, et al. Imaging of soft-tissue sarcomas with indium-111-labeled monoclonal antimyosin Fab fragments. J Nucl Med 1990;31:23–31.
18. Smith-Jones PM, Vallabhajosula S, Navarro V, Bastidas D, Goldsmith SJ, Bander NH. Radiolabeled monoclonal antibodies specific to the extracellular domain of prostate-specific membrane antigen: preclinical studies in nude mice bearing LNCaP human prostate tumor. J Nucl Med 2003;44:610–7.
19. Deb N, Goris M, Trisler K, et al. Treatment of hormone-refractory prostate cancer with 90Y-CYT-356 monoclonal antibody. Clin Cancer Res 1996;2:1289–97.
20. Epstein AL, Chen FM, Taylor CR. A novel method for the detection of necrotic lesions in human cancers. Cancer Res 1988;48:5842–8.
21. Miller GK, Naeve GS, Gaffar SA, Epstein AL. Immunologic and biochemical analysis of TNT-1 and TNT-2 monoclonal antibody binding to histones. Hybridoma 1993;12:689–98.
22. Khawli LA, Mizokami MM, Sharifi J, Hu P, Epstein AL. Pharmacokinetic characteristics and biodistribution of radioiodinated chimeric TNT-1, -2, and -3 monoclonal antibodies after chemical modification with biotin. Cancer Biother Radiopharm 2002;17:359–70.
23. Chen S, Yu L, Jiang C, et al. Pivotal study of iodine-131-labeled chimeric tumor necrosis treatment radioimmunotherapy in patients with advanced lung cancer. J Clin Oncol 2005;23:1538–47.
24. Dadachova E, Nosanchuk JD, Shi L, et al. Dead cells in melanoma tumors provide abundant antigen for targeted delivery of ionizing radiation by a mAb to melanin. Proc Natl Acad Sci U S A 2004;101:14865–70.
25. Zhao M, Beauregard DA, Loizou L, Davletov B, Brindle KM. Non-invasive detection of apoptosis using magnetic resonance imaging and a targeted contrast agent. Nat Med 2001;7:1241–4.
26. Lu CM, Burton WD, Fitzgerald RL, et al. Mass spectrometric immunoassay for parathyroid hormone-related protein. Anal Chem 2002;74:5507–12.
27. Al-Ejeh F, Darby J, Brown MP. Methods for optimizing radioimmunoconjugates and their effects on antibody activity. Cancer Biother Radiopharm 2006;21:400.
28. Pippin CG, Parker TA, McMurry TJ, Brechbiel MW. Spectrophotometric method for the determination of a bifunctional DTPA ligand in DTPA-monoclonal antibody conjugates. Bioconjug Chem 1992;3:342–5.
29. Brady ED, Chong HS, Milenic DE, Brechbiel MW. Development of a spectroscopic assay for bifunctional ligand-protein conjugates based on copper. Nucl Med Biol 2004;31:795–802.
30. Dadachova E, Chappell LL, Brechbiel MW. Spectrophotometric method for determination of bifunctional macrocyclic ligands in macrocyclic ligand-protein conjugates. Nucl Med Biol 1999;26:977–82.
31. Liu S, Edwards DS. Synthesis and characterization of two (111) In-labeled DTPA-peptide conjugates. Bioconjug Chem 2001;12:630–4.
32. Liu S, Edwards DS. Bifunctional chelators for therapeutic lanthanide radiopharmaceuticals. Bioconjug Chem 2001;12:7–34.
33. Liu S, Edwards DS. Stabilization of (90)y-labeled DOTA-biomolecule conjugates using gentisic acid and ascorbic acid. Bioconjug Chem 2001;12:554–8.
34. Liu S, Harris TD, Ellars CE, Edwards DS. Anaerobic 90Y-and 177Lu-labeling of a DOTA-conjugated nonpeptide vitronectin receptor antagonist. Bioconjug Chem 2003;14:1030–7.
35. Liu S, He Z, Hsieh WY, Fanwick PE. Synthesis, characterization, and X-ray crystal structure of In (DOTA-AA; AA=p-aminoanilide): a model for ^{111}In-labeled DOTA-biomolecule conjugates. Inorg Chem 2003;42:8831–7.
36. Liu S, Ellars CE, Edwards DS. Ascorbic acid: useful as a buffer agent and radiolytic stabilizer for metalloradiopharmaceuticals. Bioconjug Chem 2003;14:1052–6.
37. Grabarek J, Ardelt B, Kunicki J, Darzynkiewicz Z. Detection of *in situ* activation of transglutaminase during apoptosis: correlation with the cell cycle phase by multiparameter flow and laser scanning cytometry. Cytometry 2002;49:83–9.
38. Beller GA, Khaw BA, Haber E, Smith TW. Localization of radiolabeled cardiac myosin-specific antibody in myocardial infarcts. Comparison with technetium-99m stannous pyrophosphate. Circulation 1977;55:74–8.
39. Khaw BA, Fallon JT, Beller GA, Haber E. Specificity of localization of myosin-specific antibody fragments in experimental myocardial infarction. Histologic, histochemical, autoradiographic and scintigraphic studies. Circulation 1979;60:1527–31.
40. Chen FM, Taylor CR, Epstein AL. Tumor necrosis treatment of ME-180 human cervical carcinoma model with ^{131}I-labeled TNT-1 monoclonal antibody. Cancer Res 1989;49:4578–85.
41. Hornick JL, Sharifi J, Khawli LA, et al. A new chemically modified chimeric TNT-3 monoclonal antibody directed against DNA for the radioimmunotherapy of solid tumors. Cancer Biother Radiopharm 1998;13:255–68.
42. Hornick JL, Sharifi J, Khawli LA, et al. Single amino acid substitution in the Fc region of chimeric TNT-3 antibody accelerates clearance and improves immunoscintigraphy of solid tumors. J Nucl Med 2000;41:355–62.
43. Milas L, Fujii T, Hunter N, et al. Enhancement of tumor radioresponse *in vivo* by gemcitabine. Cancer Res 1999;59:107–14.
44. Lazo JS. Endothelial injury caused by antineoplastic agents. Biochem Pharmacol 1986;35:1919–23.
45. Albrecht H, DeNardo SJ. Recombinant antibodies: from the laboratory to the clinic. Cancer Biother Radiopharm 2006;21:285–304.
46. Goldenberg DM. Cancer imaging with CEA antibodies: historical and current perspectives. Int J Biol Markers 1992;7:183–8.
47. Xue LY, Butler NJ, Makrigiorgos GM, Adelstein SJ, Kassis AI. Bystander effect produced by radiolabeled tumor cells *in vivo*. Proc Natl Acad Sci U S A 2002; 99:13765–70.
48. Johnstone RW, Ruefli AA, Lowe SW. Apoptosis: a link between cancer genetics and chemotherapy. Cell 2002;108:153–64.
49. Brown JM, Attardi LD. The role of apoptosis in cancer development and treatment response. Nat Rev Cancer 2005;5:231–7.
50. Reed JC. Drug insight: Cancer therapy strategies based on restoration of endogenous cell death mechanisms. Nat Clin Pract Oncol 2006;3:388–98.
51. Bolden JE, Peart MJ, Johnstone RW. Anticancer activities of histone deacetylase inhibitors. Nat Rev Drug Discov 2006;5:769–84.

In vivo Targeting of Dead Tumor Cells in a Murine Tumor Model Using a Monoclonal Antibody Specific for the La Autoantigen

Fares Al-Ejeh, Jocelyn M. Darby, Katherine Pensa, et al.

Updated version	Access the most recent version of this article at: http://clincancerres.aacrjournals.org/content/13/18/5519s

Cited articles	This article cites 51 articles, 21 of which you can access for free at: http://clincancerres.aacrjournals.org/content/13/18/5519s.full#ref-list-1
Citing articles	This article has been cited by 3 HighWire-hosted articles. Access the articles at: http://clincancerres.aacrjournals.org/content/13/18/5519s.full#related-urls

E-mail alerts	Sign up to receive free email-alerts related to this article or journal.
Reprints and Subscriptions	To order reprints of this article or to subscribe to the journal, contact the AACR Publications Department at pubs@aacr.org.
Permissions	To request permission to re-use all or part of this article, use this link http://clincancerres.aacrjournals.org/content/13/18/5519s. Click on "Request Permissions" which will take you to the Copyright Clearance Center's (CCC) Rightslink site.